Bayesian texture classification using steerable Riesz wavelets: Application to sonar images

Alexandre Baussard[*†]
[*]ENSTA Bretagne / Lab-STICC (UMR CNRS 6285), 2 rue François Verny, 29806 Brest cédex 9, France.
[†]INP-ENSEEIHT / IRIT (UMR CNRS 5505), 2 rue Charles Camichel, 31000 Toulouse, France.
Email: alexandre.baussard@ensta-bretagne.fr

***Abstract*—In this paper, the classification and segmentation of seafloor images recorded by sidescan sonar is considered. To address this problem, which can be related to texture analysis, a supervised approach based on the Bayesian framework is proposed. The features of the textured images are obtained through a parametric probabilistic model of the 2D steerable Riesz wavelet coefficients. The generalized Gaussian distribution, which is a well-established model, is used in this contribution. It is also proposed to model the approximation coefficients using the finite Gaussian mixture model to enhance the classification rate between two statistically close classes when considering only the detail coefficients. The classification results using the 2D steerable Riesz wavelets are compared to the results obtained using the classical discrete wavelets. Then, this classification method is used for image segmentation.**

I. Introduction

The accurate characterization of texture is fundamental in various image processing applications, ranging from remote sensing to retrieval in large image databases. In this paper, the classification of textured images recorded by sidescan sonar with respect to the sea bottom types is addressed. Various approaches of this topic have been proposed and are all relying on the extraction of features from small textured images followed by a supervised or unsupervised classification [1]. Classical methods for extracting the textured seafloor information are based on first order statistics [2], on second order statistics like grey level co-occurrence matrix [3] and methods based on spectral analysis via filter banks or transforms (Gabor filters, wavelet transforms, Fourier transform...) [4]. Other approaches also exist as proposed for example in [5], [6].

In an other hand, numerous works for texture analysis have been proposed using multi-scale/multi-orientation image representations. Wavelet transforms have shown to be an effective tool to characterize texture information. The conventional scheme for texture analysis consists of representing each wavelet subband by a parametric probabilistic model that represents the marginal statistics of subbands [7]. The Generalized Gaussian distribution (GGD) is widely used to model wavelet coefficients [8] because of the almost heavy tailed aspect of the empirical probability density functions (PDF) of subbands. Several studies have considered the GGD as *a priori* knowledge of wavelet subbands statistics, leading to good results in different applications such as image retrieval, image denoising, change detection...

Following these works, a classification approach based on the statistical modeling of the wavelet subbands (detail coefficients) has been proposed for seafloor classification in [9]. The univariate GGD and the Gaussian copula based multivariate generalized Gaussian model (GC-MGG) were used and compared. In this contribution the recent 2D steerable Riesz wavelets [10] are investigated as a more powerful domain transform to extract the texture features (estimated parameters of the distributions). Basically, the classification procedure remain the same, but instead of using the classical discrete wavelet transform, the 2D steerable Riesz wavelets are used. Moreover, to enhance the classification results, the statistics of the approximation coefficients are taken into account through a finite Gaussian mixture model (MoG). This leads to efficiently separate the 'silt' and 'sand' classes which visually have the same statistics except for the luminance levels. Finally, the proposed classification method is used for image segmentation.

The sequence of the paper is organized as follows. Section II give a short overview of the 2D steerable Riesz wavelets. Section III introduces the Bayesian classification framework, the GGD and the MoG models and the similarity measures. The classification results are provided in section IV. Section V introduces the segmentation procedure and the results obtained with some samples of sonar images. Finally, section VI gives some concluding remarks.

II. 2D Steerable Riesz Wavelets

In this section a brief introduction to the 2D steerable Riesz wavelets concepts is proposed. We refer the reader to [10] for a complete theoretical presentation.

A. Riesz transform

The Riesz Transform (RT) is an extension of the Hilbert transform to two or more dimensions that has been recently introduced in signal processing to define the monogenic signal [11] as a 2D generalization of the analytic signal. In what follows, the definition from [10] is used. It combines the usual x and y components of the 2D Riesz transform into a single complex signal. The Fourrier-domain definition of the transform is

$$\mathcal{R}f(x) \overset{\mathcal{F}}{\longleftrightarrow} \frac{\omega_x + j\omega_y}{||\omega||}\hat{f}(\omega) = \mathrm{e}^{j\theta}\hat{f}_{pol}(\omega,\theta), \qquad (1)$$

where $\hat{f}(\omega) = \int_{\mathbb{R}^2} f(x)\mathrm{e}^{j<\omega,x>}\mathrm{d}x\mathrm{d}y$ with $\omega = (\omega_x, \omega_y)$ and $\hat{f}_{pol}(\omega,\theta) = \hat{f}(\omega\cos\theta, \omega\sin\theta)$ are the Cartesian and polar representations of the 2D Fourier transform of $f \in L_2(\mathbb{R}^2)$, respectively. θ is the angular frequency variable.

The n-th order (complex) RT, noted $\mathcal{R}^n$, is the n-fold iterate of $\mathcal{R}$. The RT and higher-order RT are unitary operators that are translation and scale invariant.

978-0-933957-43-5

B. Steerable Riesz wavelets

To construct steerable wavelets, it is proposed in [10] to introduce the multiorder generalized Riesz transform. It is the scalar to M-vector signal transformation $\mathbf{R}_{\mathbf{U_{M,N}}} f(x)$ whose m-th component is given by

$$\left[\mathbf{R}_{\mathbf{U_{M,N}}} f(x)\right]_m = \sum_{n=-N}^{N} u_{m,n} \mathcal{R}^n f(x), \tag{2}$$

where $\mathbf{U}_{M,N}$ is a weighting matrix.

This multiorder generalized RT, which is translation and scale invariant, can be used to map a primal isotropic wavelet frame of $L^2(\mathbb{R}^2)$, $\{\psi_{i,\mathbf{k}}\}_{i\in Z, \mathbf{k}\in Z^2}$, into a steerable wavelet frame $\{\psi_{i,\mathbf{k}}^{(m)}\}_{m=1,\ldots,M; i\in Z, \mathbf{k}\in Z^2}$ of $L^2(\mathbb{R}^2)$:

$$\psi_{i,\mathbf{k}}^{(m)} = \sum_{n=-N}^{N} u_{m,n} \mathcal{R}^n \psi_{i,\mathbf{k}}. \tag{3}$$

Thus, a primary isotropic bandlimited wavelet is required. Among the possible existing solutions, the Simoncellis wavelet appear to be a good candidate.

The 2D steerable wavelets are parametrized by the rectangular matrix $\mathbf{U}$. They are self-reversible and polar separable in the Fourier domain. Finally, they can be implemented thanks to a fast filterbank.

III. Classification within the Bayesian framework

A. Overview

Let us consider N classes $C_1, \ldots, C_N$ and $\mathbf{w} = (w_1, \ldots, w_L)$ an observation to be classified ; in our study $\mathbf{w}$ denotes coefficients from a wavelet subband. By associating a class indicator variable $Y \in \{1, \ldots, N\}$ to class indexes, the optimal decision rule that minimizes the probability of the misclassified images is given by:

$$\texttt{Class}(\mathbf{w}) = \underset{i=1,\ldots,N}{\operatorname{argmax}} \; P(Y = i \mid \mathbf{w}). \tag{4}$$

It is the Maximum *A Posteriori* probability (MAP) based decision rule. Using Bayes rule, we have

$$P(Y = i \mid \mathbf{w}) = \frac{P(\mathbf{w} \mid Y = i) P(Y = i)}{P(\mathbf{w})}. \tag{5}$$

Under the assumption that all prior class probabilities $P(Y = i)$, $i = 1, \ldots, N$, are equal, it was demonstrated in [12] that the decision rule, Equation (4), is asymptotically equivalent to minimizing the Kullback-Leibler divergence between the evidence probability $P(\mathbf{w})$ and the likelihood $P(\mathbf{w} \mid Y = i)$. In addition, in the *parametric* approach, probabilities are modeled by a member of a family of PDFs: $P(\mathbf{w}) \sim P(w; \theta_w)$ and $P(\mathbf{w} \mid Y = i) \sim P(w; \theta_i)$; in this case the decision rule in Equation (4) becomes:

$$\text{Class}(\mathbf{w}) = \underset{i=1,\ldots,N}{\operatorname{argmin}} \; \text{KLD}\left(P(w; \theta_w) \parallel P(w; \theta_i)\right), \tag{6}$$

where

$$\text{KLD}\left(P(w; \theta_w) \parallel P(w; \theta_i)\right) = \int_{-\infty}^{+\infty} P(w; \theta_w) \ln \frac{P(w; \theta_w)}{P(w; \theta_i)} \, \text{d}w. \tag{7}$$

B. Parametric probabilistic models

A conventional scheme for texture retrieval or classification consists in transforming the image into the wavelet domain and then using parametric probabilistic models that represent the marginal statistics of the detail subbands (or wavelet subbands). In this contribution, this scheme is considered but using the 2D steerable Riesz wavelets.

The usual model considered with wavelets is the Generalized Gaussian Distribution (GGD) [7], [8]. This model is also suitable for modeling the distribution of the 2D steerable Riesz wavelet coefficients in each subband for the considered sonar images. We also consider in what follows the Mixture of Gaussian model (MoG) which will be used to model the approximation coefficients. Indeed, we will show that adding these features leads to enhanced the classification rate between the ‘Sand’ and ‘Silt’ classes (which are visually close - see Figure 1) .

1) Generalized Gaussian model: The GGD is widely used to model wavelet coefficients because of the almost heavy tailed aspect of the empirical probability density functions (PDFs) of subbands [7]. It is defined by

$$f_X(x) = \frac{\beta}{2\alpha\Gamma(1/\beta)} \exp\left[-\left(\frac{|x|}{\alpha}\right)^{\beta}\right], \qquad x \in \mathbb{R} \tag{8}$$

where α and β are the parameters of the distribution and Γ is the Gamma function. α stands for the width of the PDF peak (also called the scale parameter), while β is inversely proportional to the decreasing rate of the peak (also called the shape parameter). These two parameters are estimated from the maximum likelihood estimation [13] using the Newton-Raphson method [7].

2) Gaussian mixture model: Let X be a Gaussian mixture random process. The associate probability density function is given by [14]:

$$f_X(x) = \sum_{i=1}^{n_c} \gamma_i \frac{\exp\left[-\frac{|x-\mu_i|^2}{2\sigma_i^2}\right]}{\sigma_i\sqrt{2\pi}}, \tag{9}$$

where n_c is the number of component Gaussian densities. The i_{th} component is characterized by the normal distribution with weight γ_i, mean μ_i and standard deviation σ_i.

C. Probabilistic similarity measurement

The computation of the Kullback-Leibler Divergences (KLD), to measure similarity between the two previous PDFs, is given in this part.

1) Similarity measure between two GGD PDFs: The KLD is a probabilistic metric related to the Bayesian classification. However, it has been shown that Jeffrey’s divergence (JD) can be more suitable for image retrieval or classification [15]. In fact, the KLD is asymmetric and JD (i.e. the sum of double-sided KLDs) is its symmetrized version. Moreover, it is numerically stable. Thus, the JD is considered as a similarity measurement for the GGD and also the GC-MGG.

The JD between two GGD distributions $f_X(x; \alpha_1, \beta_1)$ and $g_X(x; \alpha_2, \beta_2)$ is [7]:

$$\begin{aligned} JD(f_X | g_X) \quad &= \quad \left(\frac{\alpha_1}{\alpha_2}\right)^{\beta_2} \frac{\Gamma\left(\frac{\beta_2+1}{\beta_1}\right)}{\Gamma\left(\frac{1}{\beta_1}\right)} \\ &+ \quad \left(\frac{\alpha_2}{\alpha_1}\right)^{\beta_1} \frac{\Gamma\left(\frac{\beta_1+1}{\beta_2}\right)}{\Gamma\left(\frac{1}{\beta_2}\right)} - \frac{1}{\beta_1} - \frac{1}{\beta_2}, \end{aligned} \tag{10}$$

where $\Gamma(.)$ is the Gamma function.

2) Similarity measure between two MoG PDFs: Let $f_X(x;\omega_{i,1},\mu_{i,1},\sigma_1)$ and $g_X(x;\omega_{i,2},\mu_{i,2},\sigma_2)$, with $i=1,...,n_c$, be two MoG distributions. As a KLD expression does not exist, the approximation proposed by [16] has been used:

$$KLD(f_X|g_X) \approx \sum_{i=1}^{n_c} \omega_{i,1} \frac{\sum_{j=1}^{n_c} \omega_{j,1} e^{-D(f_i|f_j)}}{\sum_{k=1}^{n_c} \omega_{k,2} e^{-D(f_i|g_k)}}, \qquad (11)$$

where $D(f_i|f_j)$ and $D(f_i|g_k)$ are the KLD between the Gaussian components of the MoG. They are given by

$$D(f_i|f_j) = 0.5\left[\ln\left(\frac{\sigma_{j,1}^2}{\sigma_{i,1}^2}\right) + \frac{\sigma_{i,1}^2}{\sigma_{j,1}^2} - 1 + \frac{(\mu_{i,1}-\mu_{j,1})^2}{\sigma_{j,1}^2}\right], \qquad (12)$$

$$D(f_i|g_k) = 0.5\left[\ln\left(\frac{\sigma_{k,2}^2}{\sigma_{i,1}^2}\right) + \frac{\sigma_{i,1}^2}{\sigma_{k,2}^2} - 1 + \frac{(\mu_{i,1}-\mu_{k,2})^2}{\sigma_{k,2}^2}\right]. \qquad (13)$$

IV. CLASSIFICATION RESULTS

A. Database

To test the proposed classification method, a database (see Figure 1) has been compiled from Klein 5500 data recorded during the Battlespace Preparation Campaign carried out by the SACLANT Undersea Research Center in La Spezia, Italy.

To construct the database, sonar images have been manually segmented into six seafloor classes: 'Rock', 'Silt', 'Sand', 'Posidonia', 'Vertical ripples' and orientated ripples noted 45 ripples. Using these masks, small images (200x200 pixels) have been extracted. Finally, 60 images characterized by various incident angles and scaling (of the structures) have been selected for each class. Of course, we did not select the images according to the final classification results.

Note that two classes of ripples are considered here to illustrate the potential of the proposed approach to separate oriented textures (for possible other applications). This two classes will be fused in what follows for some numerical results and for the image segmentation task.

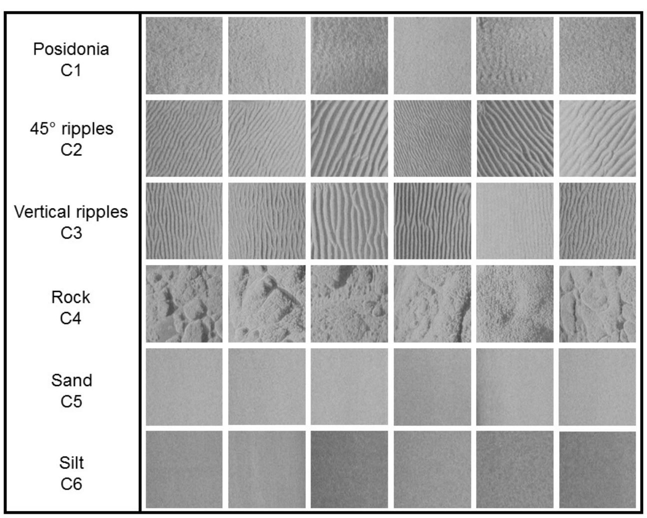

Fig. 1. Examples of sonar texture images extracted from the database.

B. Classification results using the GGD model

Table I gives the percentage of good classification corresponding to the averaging of 100 realizations. Indeed, for each considered ratio the training and the test sets are randomly determined from the database. It is also provided the standard deviation of the obtained classification results. These results show that considering the 2D steerable Riesz wavelets (SWT) instead of the common discrete wavelets (DWT) leads to better classification results.

	DWT-GGD	SWT-GGD
1/2	94.24 ± 3.83	95.52 ± 3.47
1/3	92.95 ± 3.95	94.33 ± 3.64
1/4	91.70 ± 4.53	93.47 ± 4.03
1/8	87.41 ± 6.55	89.27 ± 6.64

TABLE I. CLASSIFICATION RESULTS FOR SEVERAL RATIOS BETWEEN THE TRAINING AND THE TEST SETS CONSIDERING THE GGD TO MODEL THE STATISTICS OF THE DISCRET WAVELET (DWT) AND THE STEERABLE RIESZ WAVELET (SWT) SUBBANDS.

If we take a closer look at the confusion matrix for the ratio equal to 1/3 given in Table II, one can note that the classification results are mainly damaged by the confusion between the C5 and C6 classes and between C2 and the two other classes C1 and C3. In what follows we provide some analysis about the confusion between C5 and C6 and propose a solution to overcome it.

	C1	C2	C3	C4	C5	C6
C1	97.25	0	0	0.63	0	2.12
C2	5.00	83.95	4.95	3.73	0	2.37
C3	0	1.62	96.60	0	1.30	0.48
C4	2.12	0.15	0	97.73	0	0
C5	0	0	0	0	88.65	11.35
C6	0.15	0	0	0	6.33	93.52

(a)

	C1	C2	C3	C4	C5	C6
C1	97.55	0	0	0.1	0	2.35
C2	4.08	88.65	2.20	4.05	0	1.02
C3	0.05	0.70	98.03	0	0	1.22
C4	2.23	0.2	0	97.58	0	0
C5	0	0	0	0	90.85	9.15
C6	0.27	0	0	0	6.38	93.35

(b)

TABLE II. CONFUSION MATRICES FOR (A) THE DWT-GGD AND (B) THE SWT-GGD APPROACHES FOR A RATIO EQUAL TO 1/3.

C. 'Sand' and 'Silt' classes

As shown in the previous section through the confusion matrices, one of the strongest losses of good classification comes from the 'Sand' and 'Silt' classes. As can be seen in Figure 1, these two classes are visually really close. The main difference appears to be at least the luminance.

The comparison of the estimated GGD for each subband show that in the wavelet domain these two classes remain close (similar distributions). In order enhance the classification rate, we propose in this contribution to take into account the distribution of the approximation coefficients. Indeed, the corresponding estimated distributions using a finite Gaussian mixture model (with 4 components), appear to have very different means and shapes. Thus, taking into account these features in the classification process could lead to enhance the classification rate between both classes. Note that in what follows the estimation of the MoG parameters is based on [14] and can be easily done thanks to Matlab functions.

D. Classification results using the GGD and the MoG models

According to the previous comments, we propose taking into account the approximation coefficients in our classification process to be able to separate the classes C5 and C6. There are several ways to include these features during the classification process.

After some simulations, we finally use a classification procedure based on two steps:

S1- Process a first classification using only the GGD features (same as in the previous section).

S2- Process a second classification considering the images classified during S1 as 'Sand' and 'Silt'. In this step, for the training set and the tested images, the feature vectors are made of the GGD and MoG parameters.

Note that considering the GGD and MoG features for all the classes in an one step process leads to damage the classification rate.

The new classification results are given in Table III. They show enhancement of the classification rates, comparing to Table I. This is also illustrated, for the SWT, in the new confusion matrix given in Table IV. As expected, this two steps classification process leads to efficiently separate the 'Sand' and 'Silt' classes.

	DWT-GGD+MoG	SWT-GGD+MoG
1/2	96.91 ± 2.44	97.75 ± 2.18
1/3	95.85 ± 2.59	96.82 ± 2.35
1/4	94.84 ± 3.40	95.95 ± 2.98
1/8	91.67 ± 4.43	92.46 ± 4.61

TABLE III. COMPARISON OF THE CLASSIFICATION RESULTS FOR SEVERAL RATIOS BETWEEN THE TRAINING AND TEST SETS CONSIDERING THE GGD+MOG MODEL.

	C1	C2	C3	C4	C5	C6
C1	97.55	0	0	0.1	0	2.35
C2	4.08	88.65	2.20	4.05	0	1.02
C3	0.05	0.70	98.03	0	0	1.22
C4	2.23	0.2	0	97.58	0	0
C5	0	0	0	0	99.40	0.60
C6	0.27	0	0	0	0	99.73

TABLE IV. CONFUSION MATRIX FOR THE SWT-GGD+MOG APPROACH FOR A RATIO EQUAL TO 1/3.

V. APPLICATION TO IMAGE SEGMENTATION

A. Description

In this last section, we investigate the previous classification method for image segmentation. Following [17], the segmentation scheme simply consists to move a square block centered on each pixel (or using a sliding step) of the image. The label of the current pixel corresponds to the classification result of the patch image in the square block.

In practical seabed classification/segmentation, the ripples are generally not classified into several classes according to their orientations (indeed they can have any orientation). Thus, we have fused the two ripples classes into one by selecting randomly 30 images in both classes. The confusion matrix for a ratio equal to 1/3 is given in Table V. The classification rate obtained is 96.81±2.85. This result is close to the result using 6 classes meaning that fusing the two classes do not enhance or damage the classification results.

	C1	C2 & C3	C4	C5	C6
C1	97.53	0	0.4	2.07	0
C2 & C3	4.58	89.65	4.10	1.52	0.15
C4	1.33	0	98.67	0	0
C5	0	0	0	98.90	1.10
C6	0.55	0	0	0.15	99.30

TABLE V. CONFUSION MATRIX FOR THE DATABASE CONSIDERING ONLY ONE CLASS OF RIPPLES USING THE SWT-GGD+MOG MODEL FOR A RATIO EQUAL TO 1/3.

Before applying the segmentation process to a sonar image, we also study if the classification results change according to the size of the images. Indeed, the 'resolution' of the segmented image will depend on the size of the sliding windows (i.e. the size of the images in the database). Thus, we extract from the database two new databases made of 64×64 and 32×32 pixels patches. The confusion matrices obtained are given in Table VI and VII. The global classification rates are 96.07±2.26 for the 64×64-sized patches (using the DWT the result is 94.07±2.36) and 74.51±2.05 for the 32×32-sized patches. From these results, one can note that the classification results with the 64×64-sized images are very similar to the classification results obtained with the images with size 200×200 pixels. Thus, one can expect efficient segmentation results. Moreover, with the 32×32-sized images there are too much confusions between classes. For this size, the data can not be efficiently modeled by the considered distributions (or too few data).

	C1	C2 & C3	C4	C5	C6
C1	94.36	0	1.30	4.27	0.07
C2 & C3	1.03	97.59	1.07	0.31	0
C4	6.09	0.27	93.48	0.01	0.15
C5	0.38	0	0.06	97.80	1.76
C6	2.38	0	0.02	0.50	97.10

TABLE VI. CONFUSION MATRIX FOR THE DATABASE MADE OF 5 CLASSES OF IMAGES WITH 64×64 PIXELS, USING THE SWT-GGD+MOG MODEL AND FOR A RATIO EQUAL TO 1/3.

	C1	C2 & C3	C4	C5	C6
C1	75.55	1.23	10.98	5.92	6.32
C2 & C3	10.14	76.87	11.00	1.28	0.71
C4	19.33	2.86	75.71	0.85	1.25
C5	1.83	0.02	0.35	79.47	18.33
C6	5.53	0.54	0.38	28.58	64.97

TABLE VII. CONFUSION MATRIX FOR THE DATABASE MADE OF 5 CLASSES OF 32×32-PIXELS IMAGES, USING THE SWT-GGD+MOG MODEL AND FOR A RATIO EQUAL TO 1/3.

B. Segmentation results

In this contribution 4 samples of sonar images are used to illustrate the potential of the proposed method for image segmentation. Unfortunately, we do not have the ground truth, but one can visually give qualitative analysis of the results.

The considered sample images have been chosen so that they can be considered representative of seafloor images. Figures 2, 3, 4 and 5 show the original image and the corresponding segmentation results. On can note that some pixels are mislabelled, especially those at the border of two areas. This is probably due to a blocking effect. Indeed, the distribution parameters at a given pixel are estimated with wavelet coefficients from surrounding pixels, but data in this block do not belong to a single class because of the block size. Finally, one can also note that it is possible to add post-processing in order to smooth the results (remove spots of mislabelled pixels).

VI. CONCLUDING REMARKS

In this contribution the 2D steerable Riesz wavelets have been investigated to classify textured images extracted from sidescan sonar images. The Bayesian framework has been used with parametric models based on the generalized Gaussian distribution and the finite Gaussian mixture. We also provide an extension of this approach to image segmentation. The numerical simulations show enhancement in the classification results in comparison with the classical approach based on the discrete wavelet transform. The silt and sand classes have been also efficiently separated thanks to the proposed two steps classification process. The first segmentation results show the potential and the limitations of the proposed approach. Indeed, it remains confusions between some classes and we have to investigate better solutions to manage the misclassification which can appear at the junction of two areas.

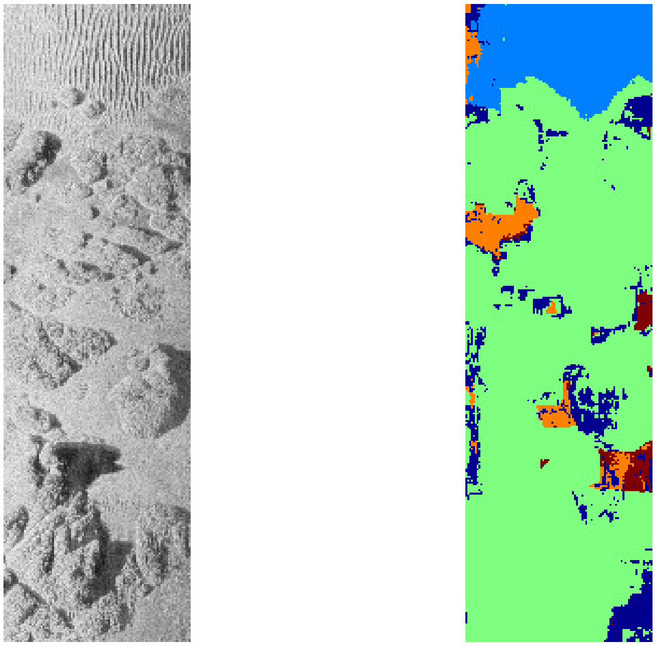

Fig. 2. Example 1 of a sonar image and the segmentation result.

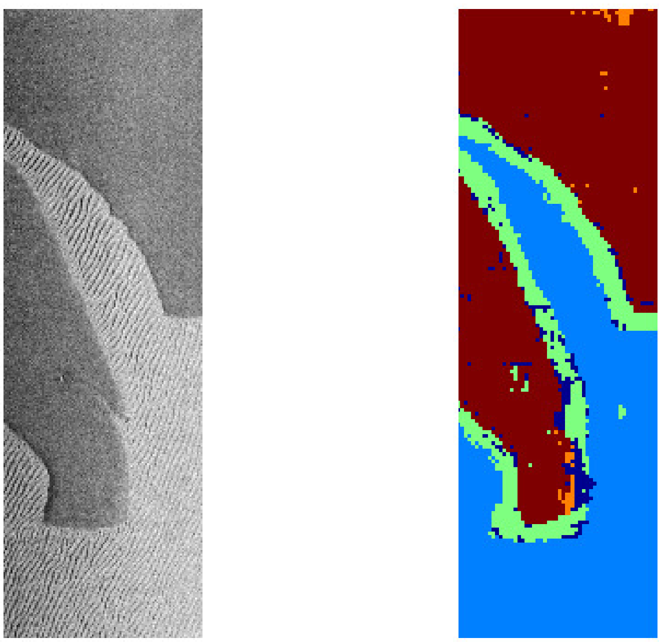

Fig. 3. Example 2 of a sonar image and the obtained segmentation.

ACKNOWLEDGMENT

This work was supported by DGA/MRIS. The data were provided by DGA/TN Brest.

REFERENCES

[1] N. Valeyrie, Y. Pailhas, C. Capus, and Y. Petillot, "Texture recognition in synthetic aperture sonar images with scattering operators," in *4th International Conference and Exhibition on Underwater Acoustic Measurements: Technologies & Results*, Kos, 2011.

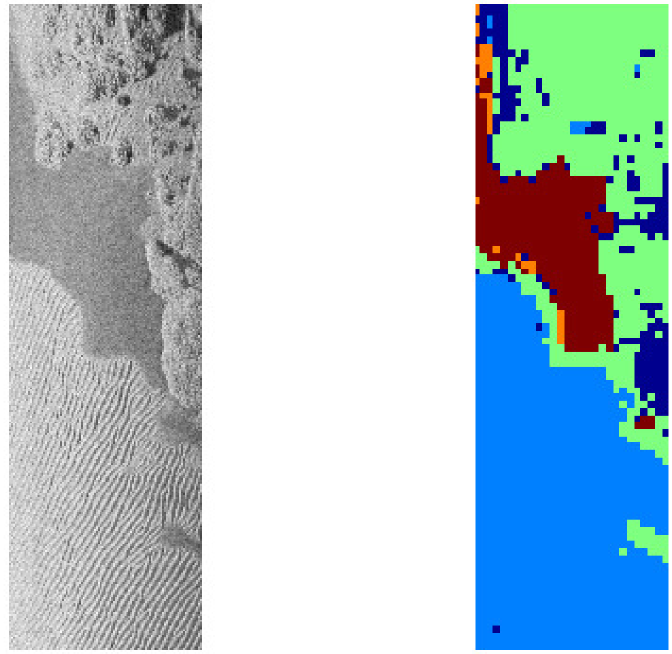

Fig. 4. Example 3 of a sonar image and the segmentation result.

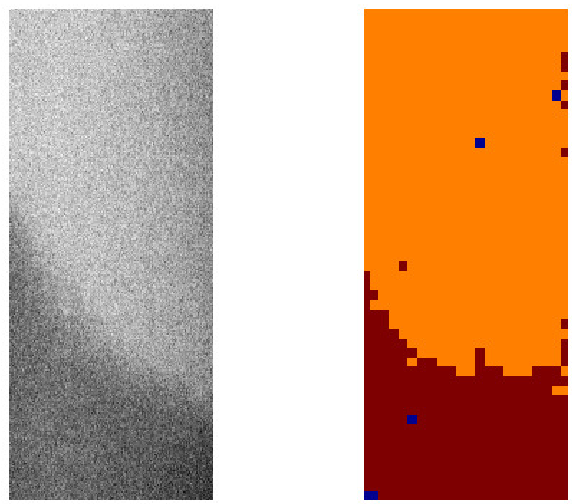

Fig. 5. Example 4 of a sonar image and the segmentation result.

[2] G. Le Chenadec and J.-M. Boucher, "Sonar image segmentation using the angular dependence of backscattering distributions," in *Proceedings of IEEE/MTS OCEANS*, Brest, 2005.

[3] I. Karoui, R. Fablet, J.-M. Boucher, and J.-M. Augustin, "Seabed segmentation using optimized statistics of sonar textures," *IEEE Journal of Oceanic Engineering*, vol. 47, no. 6, pp. 1621–1631, 2009.

[4] A. Nait-Chabane, B. Zerr, and G. Le Chenadec, "Spectral directional filter bank for sidescan sonar segmentation with unsupervised neural network approach," in *International Conference and Exhibition on Underwater Acoustics*, Corfu, 2013.

[5] H.-G. Nguyen, R. Fablet, A. Ehrhold, and J.-M. Boucher, "Keypoint-based analysis of sonar images: Application to seabed recognition," *IEEE Transactions on Geoscience and Remote Sensing*, vol. 50, no. 4, pp. 1171–1184, 2011.

[6] D. P. Williams, "Bayesian data fusion of multiview synthetic aperture sonar imagery for seabed classification," *IEEE Transactions on Image Processing*, vol. 18, no. 6, pp. 1239–1254, 2009.

[7] M. Do and M. Vetterli, “Wavelet-based texture retrieval using generalized Gaussian density and Kullback-Leibler distance,” *IEEE Transactions on Image Processing*, vol. 11, no. 2, pp. 146–158, 2002.

[8] S. Mallat, “A theory for multiresolution signal decomposition: the wavelet representation,” *IEEE Transactions on Pattern Analysis and Machine Intelligence*, vol. 11, no. 7, pp. 674–693, 1989.

[9] N.-E. Lasmar, A. Baussard, and G. Le Chenadec, “Seafloor classification using statistical modeling of wavelet subbands,” in *2nd International Conference & Exhibition on Underwater Acoustics*, Rhodes, 2014.

[10] M. Unser and N. Chenouard, “A unifying parametric framework for 2D steerable wavelet transforms,” *SIAM Journal of Imaging Sciences*, vol. 6, no. 1, pp. 102–135, 2013.

[11] M. Felsberg and G. Sommer, “The monogenic signal,” *IEEE Trans. Signal Processing*, vol. 49, no. 12, pp. 3136–3144, 2001.

[12] N. Vasconcelos and A. Lippman, “A probabilistic architecture for content-based image retrieval,” in *Proceedings IEEE Conference on Computer Vision and Pattern Recognition - CVPR*, 2000, pp. 216–221.

[13] M. Varanasi and B. Aazhang, “Parametric generalized gaussian density estimation,” *Journal of the Acoustical Society of America*, vol. 86, no. 4, pp. 1404–1415, 1989.

[14] G. McLachlan and D. Peel, *Finite mixture models*. Wiley series in Probability and Statistics, 2005.

[15] H. Liu, D. Song, S. Ruger, R. Hu, and V. Uren, “Comparing dissimilarity measures for content-based image retrieval,” *Information Retrieval Technology*, vol. 4993, pp. 44–50, 2008.

[16] J. R. Hershey and A. Peder, “Approximating the Kullback Leibler divergence between gaussian mixture models,” in *IEEE International Conference on Acoustics, Speech and Signal Processing*, 2007.

[17] Y. Peng, X. Xu, W. Zhou, and Y. Zhao, “SAR image classification based on alpha-stable distribution,” *Remote Sensing Letters*, vol. 2, no. 1, pp. 51–59, 2011.